

## COMPUTATIONAL FLUID DYNAMICS (CFD) SIMULATIONS OF AEROSOL DEPOSITION IN THE LUNGS

**Pantelis G. Koullapis and Stavros C. Kassinos**

Computational Sciences Laboratory (UCY-CompSci)  
Department of Mechanical and Manufacturing Engineering  
University of Cyprus, University Avenue 1, 2109 Nicosia, Cyprus  
kassinos@ucy.ac.cy

**Ching-Long Lin**

Department of Mechanical and Industrial Engineering, and IIHR-Hydroscience and Engineering,  
The University of Iowa, Iowa City, Iowa 52242

### ABSTRACT

In the current study, Large Eddy Simulations (LES) are used to investigate the transport and deposition of inhaled aerosol particles ( $d_p = 0.1, 0.5, 1, 2.5, 5, 10 \mu\text{m}$ ) in a realistic geometry of the human airways under steady inhalation. The effects of electrostatic charge and lower generation airway narrowing caused by Chronic Obstructive Pulmonary Disease (COPD) on particle transport and deposition are examined for various flowrates (sedentary - 15.2 lt/min, light - 30 lt/min and heavy activity - 60 lt/min). Results show that the mean flow structures at the three flowrates are qualitatively similar regardless of Reynolds number. Similar swirling motions are generated from the impingement of the laryngeal jet on the tracheal front wall. However, higher turbulence intensities that persist further downstream in the trachea and the main bronchi are observed as the flowrate is increased. The Deposition Efficiency (DE) of particles is increased with the flowrate due to greater inertial impaction. The majority of the larger particles are filtered in the mouth-throat region, while 0.1, 0.5 and 1  $\mu\text{m}$  diameter particles have similar DE at a given flowrate. The effect of charge on DE of particles is more pronounced for smaller particles; 1000 elementary charge units on 0.1, 0.5, 1 and 2.5  $\mu\text{m}$  diameter particles results in approximately 7, 3, 2.5 and 1.5 times greater overall DE than that with no charge, respectively. Obstructed lower generation airways result in enhanced deposition due to impaction caused by higher velocities in these airways.

### INTRODUCTION

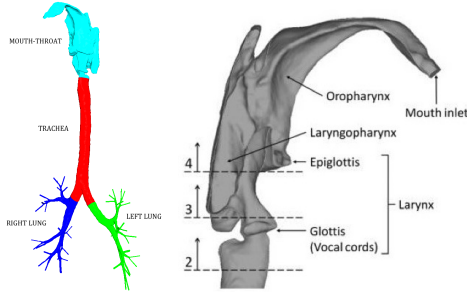
Computational Fluid Dynamics (CFD) techniques are being increasingly used to simulate flow behavior in the human respiratory system. Recent works include Reynolds Averaged Navier-Stokes (RANS) simulations (Luo & Liu, 2008), Large Eddy Simulations (LES) (Choi *et al.* (2009), Radhakrishnan & Kassinos (2009)) and Direct Numerical Simulations (DNS) (Lin *et al.*, 2007). Both idealized model geometries and geometries obtained from medical imaging have been used. The deposition of therapeutic or pollutant xenobiotic particles is dependent on the characteristics of the respiratory flow by which they are transported (Xi &

Longest, 2007). The ultimate goal of the application of CFD techniques is an in-depth understanding of the fate of inhaled pollutants, including deposition and possible mucus clearance, as well as the efficient pulmonary delivery of drugs targeting respiratory or systemic diseases.

An important parameter affecting both the characteristics of the airflow and particle transport is the inhalation rate. A higher flowrate causes an earlier transition to turbulence and higher overall turbulence levels. Johnstone *et al.* (2004) studied experimentally the velocity fields in an idealized model of the human extrathoracic airway during steady inspiration and found that Reynolds stress profiles were highly dependent on inhalation flowrate, especially in the separated shear layer regions. Flow rates of 15, 30 and 60 lt/min are considered to correspond to sedentary, light and heavy activity conditions, respectively (Xi & Longest, 2007).

In drug delivery applications, medical devices such as nebulisers, Metered Dose Inhalers (MDI) and Dry Powder Inhalers (DPI) often generate electrostatically charged aerosols (Kwok (2005), Kwok & Chan (2009)). In addition, pollution aerosols generated in the environment or in occupational settings, may have charges well above the Boltzmann equilibrium level. Thus, consideration of electrostatic particle properties must be taken into account in human health risk assessments (Forsyth, 1998). Theoretical studies in lung models (Yu, 1985), experiments in man (Prodi, 1985) and clinical measurements confirmed that charge carried by particles enhances the deposition of the particles in the lung considerably. This is not desirable for drugs intended for systemic uptake, which must pass into the blood through the alveolar epithelium and thus early deposition is unwanted, but might be desirable for drug delivery in certain upper regions of the airway tree or even leveraged for the removal of pollutant particles using electrostatic charge effects (Ali, 2008).

Chronic Obstructive Pulmonary Disease (COPD) is a common and life-threatening condition, causing high morbidity and mortality in industrialized countries (Hea, 2008). COPD is characterized by airflow obstruction that is not fully reversible, caused by airway narrowing resulting from the combination of increased mucus, excess tissue, and in-



(a) Full geometry (b) Inside oblique view of the and sub-regions. upper airways.

Figure 1: Realistic human airway tree geometry (provided to us by the Department of Mechanical and Industrial Engineering of the University of Iowa, USA (Choi *et al.*, 2009)).

flammation. The reduction is less pronounced in the large airways because morphological structures (such as muscle tone and cartilaginous rings) maintain the rigidity of these airways. Experimental studies have shown that total lung deposition of inhaled particles is much greater in patients with obstructive airway disease such as asthma and COPD compared to healthy individuals (Kim & Kang, 1997). The deposition enhancement in the patient is generally confined to the central airway regions, indicating a critical role of obstructed airways in deposition enhancement.

The aim of this study is to quantitatively assess the distinct effects of inhalation flowrate, aerosol charge and airway obstruction on particle deposition enhancement in a realistic geometry of the human respiratory system using LES and Euler-Lagrangian approach. In the cases of different flowrate, the airflow characteristics are also examined.

## AIRWAY GEOMETRY

The physical domain in which flow is simulated can be simplified by representing the airways as smooth circular cylinders, e.g. the symmetric model of Weibel (1965). With recent advancements in medical imaging and computer technologies, it is now possible to reconstruct the human respiratory tract from Multi-Detector Computed Tomography scans and compute airflow in domains that are patient specific and anatomically accurate. The geometry considered in this study is shown in Fig. 1 and it represents a non-smoking 20 year old female. The respiratory tract includes the extrathoracic airways of the mouth, the oropharynx, the laryngopharynx, the larynx and the trachea as well as the intrathoracic airways up to generation 7 (resolution limitations restrict further CT-reconstruction of lower airway generations). Table 1 summarizes the geometrical (cross-sectional areas and hydraulic diameters) and flow (average velocities and Reynolds numbers) properties on the cross-sections of interest for the three flowrates considered in this study.

The modification of particle deposition characteristics due to disease-induced airway obstruction is emulated through the reduction of the diameters of the lowest generation airways of the initial geometry. Hasegawa (2006) used three-dimensional computed tomography and demonstrated that airflow limitation in COPD is more closely related to the dimensions of the distal (small) airways than proximal (large) airways. Based on this finding, the dimensions of

the upper airways (extrathoracic region) were left the same in our obstructed airway model. Starting from the middle of the trachea, the airway luminal area was gradually decreased as one moves to the lower generations, reaching the value specified by a scaling factor,  $\alpha = d_0/d = 1.5$ , at the lowest generation airways.

Table 1: Geometrical and flow properties on the cross-sections of interest.

Cross section	A(mm <sup>2</sup> )/ Dh(mm)	U	Re
		= $\frac{Q}{A}$ (m/s)	= $\frac{U D}{\nu} = \frac{2Q}{\nu D}$
		$\dot{Q}=15.2 / 30 / 60$ lt/min	$\dot{Q}=15.2 / 30 / 60$ lt/min
Midpharynx	401 / 22.6	0.630 / 1.247 / 2.494	838 / 1654 / 3308
Glottis	39.3 / 7.074	6.43 / 12.725 / 25.45	2676 / 5084 / 10168
Trachea	157.8 / 14.2	1.6 / 3.17 / 6.34	1337 / 2639 / 5278

## NUMERICAL METHOD

### Continuous phase simulation

The airflow in the upper and conducting airways is understood to be turbulent or transitional over much of the inhalation cycle (Lin *et al.*, 2007). Thus, we are employing LES with a dynamic Smagorinsky subgrid scale model in order to study the unsteady flow in the lungs geometry. LES has been chosen because of its ability to resolve the large-scale energy containing eddies (even though it models small-unresolved scales) and to deal with regions of transitional flow in between fully turbulent flow. It is more accurate than RANS modeling, but with a significantly greater computational cost.

The airflow is described by the filtered set of incompressible Navier-Stokes equations, eqn. 1 and 2, which are solved using OpenFOAM (Open Source CFD toolbox),

$$\frac{\partial \bar{u}_j}{\partial x_j} = 0 \quad (1)$$

$$\frac{\partial \bar{u}_i}{\partial t} + \bar{u}_j \frac{\partial \bar{u}_i}{\partial x_j} = -\frac{1}{\rho} \frac{\partial \bar{p}}{\partial x_i} + \frac{\partial}{\partial x_j} \left[ (\nu + \nu_{sgs}) \frac{\partial \bar{u}_i}{\partial x_j} \right] \quad (2)$$

Here,  $\bar{u}_i$ ,  $\bar{p}$ ,  $\rho$ ,  $\nu$  and  $\nu_{sgs}$  are the velocity components in the  $i$ -direction, pressure, density, kinematic viscosity, and subgrid-scale (SGS) turbulent eddy viscosity, respectively. In the current study, the density and the kinematic viscosity of the air are  $1.2 \text{ kg/m}^3$  and  $1.7 \times 10^{-5} \text{ m}^2/\text{s}$ , respectively. The overbar denotes resolved quantities. Uniform velocity at the inlet and zero pressure at the outlets were set as boundary conditions (Luo & Liu, 2008). The discretization of the equations is done using the finite volume method and second order discretization schemes in both time and space. The PISO algorithm is employed for the treatment of the pressure-velocity system.

### Lagrangian Particle Tracking

After the flow and turbulence have developed, spherical, rigid and non rotating particles are introduced at the mouth inlet. At each time step, the flow equations are solved first and then the motion of each particle is individually computed (Lagrangian approach) by solving Newton's equations (eqn. 3) to determine the particle velocity and position,

$$m_p \frac{d\vec{u}_p}{dt} = \sum \vec{F}, \quad \frac{d\vec{x}_p}{dt} = \vec{u}_p \quad (3)$$

Here,  $\sum \vec{F}$  is the sum of forces acting on each particle, which includes the drag ( $\vec{F}_D$ ), gravity ( $\vec{F}_G$ ), Brownian ( $\vec{F}_B$ ) and electrostatic image charge forces ( $\vec{F}_{image}$ ). Brownian force is important for particles with diameter less than  $1\mu\text{m}$  while image charge force is considered for particles carrying electrostatic charges. The expression for  $\vec{F}_D$  is based on the correlation proposed by Schiller & Naumann (1935). The image charge force is the attractive force experienced by a particle with a charge  $q$  near a conducting wall,

$$\vec{F}_{image} = \frac{q^2}{16\pi\epsilon_0|\vec{r}_{p,w}|^2} \frac{\vec{r}_{p,w}}{|\vec{r}_{p,w}|} \quad (4)$$

where  $\vec{r}_{p,w}$  is the minimum distance vector between the particle and the conducting wall and  $\epsilon_0 = 8.854 \times 10^{-12} \text{ C}^2/(\text{Nm}^2)$  is the permittivity of free space. The unit vector  $\vec{r}_{p,w}/|\vec{r}_{p,w}|$  is normal to the wall surface and points away from the space occupied by the air passage, such that the image force always acts in the direction of the wall.

An implicit Euler integration scheme is employed to integrate the equations of motion. A particle is considered deposited if the shortest distance from the center of particle to the airway wall is less than the particle radius. This treatment of particle deposition is justified by the presence of the sticky mucous layer that covers the interior of the airways and whose function is to trap inhaled particles. One-way coupling is taken into account.

### Mesh sensitivity study

Two unstructured meshes with 23 (Mesh 1) and 34 (Mesh 2) million control volumes were generated using ANSYS ICFM software.

In order to examine the sensitivity of our results on mesh size, two tests were carried out at  $\dot{Q} = 30 \text{ lt/min}$ . The first test is about the distribution of the normalised mean and root-mean-squared (rms) velocity fluctuations along the jet centerline<sup>1</sup> and is shown in fig. 2. The plots show good agreement between the two meshes. The second test is carried out in order to assess the effect of grid size on overall and regional deposition efficiencies (DE) of uncharged particles ( $q=0$ ). For the regional deposition study, the geometry was divided in four sub-regions as shown in figure 1a, i.e. mouth-throat (cyan), tracheal (red), left (green) and right lung (blue). Negligible variations for the particle DE were observed between the two meshes considered. Based on the grid sensitivity study, Mesh 1 is used for the lowest flowrate of  $\dot{Q} = 15.2 \text{ lt/min}$ , while Mesh 2 is used for the higher flowrates of  $\dot{Q} = 30 \text{ lt/min}$  and  $\dot{Q} = 60 \text{ lt/min}$ .

## RESULTS AND DISCUSSION

### Flow field

In this section, we show the effects of inhalation rate (15.2, 30, 60 lt/min) on the characteristics of the flow field. In the regions of interest (oropharyngeal, laryngeal and tracheal regions), flow field differences between the healthy and diseased lungs were found to be moderate and for the sake of brevity results are shown only for the healthy lung.

Fig. 3 shows the contours and secondary component vectors of normalised mean velocities as well as the contours of normalised turbulent kinetic energy (TKE) in a vertical and three horizontal cut-planes. Fig. 3 also displays the

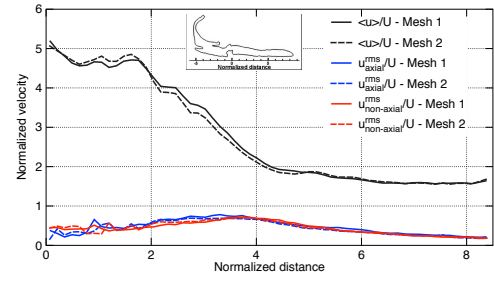


Figure 2: Distribution of the normalised mean and rms velocity fluctuations along the jet centerline at  $\dot{Q} = 30 \text{ lt/min}$  ( $U=3.17 \text{ m/s}$  is the tracheal average velocity).

velocity profiles in black at the lines of intersection of the cut-planes. For the sake of brevity results are shown for the flowrates of 15.2 and 30 lt/min (moderate flow field differences between the cases of 30 and 60 lt/min).

Mean flow structures are qualitatively similar for the three flowrates regardless of Reynolds number. The normalized mean velocity initially exhibits a high speed jet in the oral region and then decelerates when passing through the wide and curved passage of the oropharynx and the laryngopharynx. This oral jet develops in a shorter axial distance at higher Reynolds number (jet core velocity decays more rapidly), which agrees with the experimental study for circular jets of Kwon & Seo (2005). The jet entering the oral cavity causes a recirculation zone close to the anterior wall. Also, for the two higher flowrates the jet is dispersed in the oral cavity and as a result the jet impingement on the curved rear wall of the oral cavity is weakened. The different oral jet characteristics are most probably the reason behind the differences in the secondary motions in the oropharynx (slice A), observed under the various flowrates. The laryngeal jet is formed starting slightly upstream of the glottis due to the constricted cross-sectional area and it impinges on the tracheal front wall. This jetting effect creates a large recirculation zone near the dorsal wall of the upper trachea. Asymmetric counter-rotating secondary motions are generated as we move downstream in the trachea (slices B - more clear for  $\dot{Q} = 30 \text{ lt/min}$ ); fluid from the impinging laryngeal jet flows along the walls from the anterior to posterior side and then presses against it. At slice C, only one vortex is evident. The characteristics of these swirling motions are virtually independent of Re, which agrees with the experimental observations of Johnstone *et al.* (2004). Further downstream, the jet is dispersed and the secondary motions are weakened.

TKE in the oral region rises rapidly after the constriction due to the soft palate. The location of maximum TKE in this region depends on the Reynolds number; at the lower flowrate of  $\dot{Q} = 15.2 \text{ lt/min}$ , the high TKE region is located downstream of the oral jet impingement, at the entrance of oropharynx, while in the cases of the higher flowrates, TKE maximum is found upstream in the oral cavity region. This is also supported by the study of Kwon & Seo (2005), who found that turbulence intensities on the shear layers of round jets are gradually increased as the Reynolds number increases. Further downstream in the oropharynx and laryngopharynx, the TKE is suppressed due to the increased flow cross section, but it is augmented again by the glottis constriction. A high TKE region is found at the interface between the cavity-like flow in the recirculation zone and the free stream velocity. This TKE maximum is associated with

<sup>1</sup>Jet centreline is defined as the loci where the maximum mean velocity at each axial station is located.

the mixing layer formed between the jet core and the ambient air. A second region of high TKE in the trachea is located near the end of the jet core and is attributable to the transition of the jet to turbulence. These two regions extend in greater areas as Reynold number is increased. TKE is reduced as we move further downstream to the lower part of the trachea. Fig. 4 displays the contours of turbulence intensity in a vertical plane cutting through lower trachea and major bronchial airways, at the three flowrates considered. At higher flowrates, higher values of turbulent intensities are recorded that persist further downstream in the trachea as well as in the left and right main bronchi.

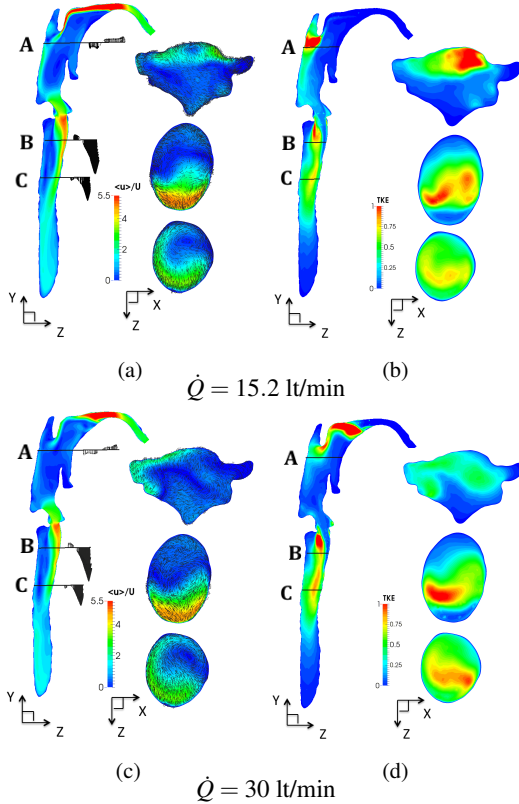


Figure 3: Contours and vectors of normalised mean velocity, (a),(c). Contours of normalised TKE, (b),(d).

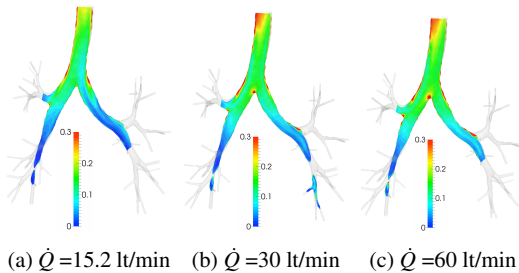


Figure 4: Contours of turbulence intensity in lower trachea and major bronchial airways.

### Particle transport and deposition

In this section, simulation results for the effects of flowrate, particle charge and airway obstruction on aerosol

transport and deposition are discussed. The particle sizes considered are: 0.1, 0.5, 1, 2.5, 5 and  $10\mu\text{m}$ .

**Effect of flowrate** Figs. 5a, b and c present the overall and regional Deposition Efficiencies (DE) of uncharged particles as a function of particle size and flowrate. Independently of the flowrate, almost all of the  $10\mu\text{m}$  particles are deposited in the mouth-throat region, as shown in fig. 6. The deposition hot spots for these particles are the upper area after the first curvature and above the tongue (hard and soft palate) as well as the rear wall of the oral cavity, known as uvula (marked by arrows in fig. 6a). In the two higher flowrate cases, the first curvature filters approximately 97% of  $10\mu\text{m}$  of these particles. In general, due to their high inertia, larger particles deviate from the fluid streamlines and impact at the curved airway walls in the mouth region. The effect of flowrate is more pronounced on the deposition of  $5\mu\text{m}$  diameter particles. Increasing the flowrate from 15.2 to 30 lt/min causes a rise in the overall and mouth-throat DE of about 40%. For this particle size, the oral jet at the uvula causes significant impaction, as shown in fig. 6. Considerable deposition also occurs on the sidewalls of the larynx immediately upstream of the glottis constriction and on the sidewalls of the upper trachea due to inertial impaction arising from the laryngeal jet and the associated secondary motions. Left and right lung DE of  $5\mu\text{m}$  particles are reduced for higher flowrates as a result of the more efficient filtering on the upper airways.  $2.5\mu\text{m}$  have overall DE below 10% for  $\dot{Q} = 15.2$  lt/min. The increase in overall (mouth-throat) DE of these particles is approximately 23% (15%) for  $\dot{Q} = 30$  lt/min and 70% (55%) for  $\dot{Q} = 60$  lt/min. As the flowrate is increased, enhanced deposition for particles of this size is observed at the uvula, upstream of the glottis constriction, on the upper tracheal walls and at the bifurcations of lower lung generations. Also the recirculation zone in the oral cavity traps some of these particles and as a result increased deposition is observed on the anterior wall of the oral cavity. While the same pattern of enhanced DE with increasing flowrate is also observed in the case of smaller  $1\mu\text{m}$  particles, in this case one can also discern the effect of Brownian diffusion. For example, the slightly larger DE in the trachea and left lung for the  $0.1\mu\text{m}$  particles, as compared to the DE of  $0.5\mu\text{m}$  ones, can be attributed to Brownian motion.

**Effect of particle charge** Electrostatic charge plays a role in the transport and deposition of both pharmaceutical aerosols generated from medical devices and pollutant aerosols. The level of charge present depends on the size and physical properties of these aerosols (larger particles can hold more charge). In order to assess the effect of charge on the deposition of particles, five charge levels, i.e. 0, 50, 250, 500 and 1000 elementary charges (e) were considered for particle sizes of 0.1, 0.5, 1, 2.5 and  $5\mu\text{m}$  at the lower flowrate of  $\dot{Q} = 15.2$  lt/min. These charge levels are below the Rayleigh charge limit, which is the maximum amount of charge a liquid droplet can carry. Fig. 7 shows the overall and sub-regional DE of particles with different charge levels ( $5\mu\text{m}$  particles are not shown due to insignificant variation in DE). We can observe that the effect of charge becomes more pronounced for smaller particle sizes; the overall DE of  $0.1\mu\text{m}$  with 1000 elementary charges is approximately 7 times greater than that with no charge. However, 1000e is exactly the Rayleigh limit for  $0.1$

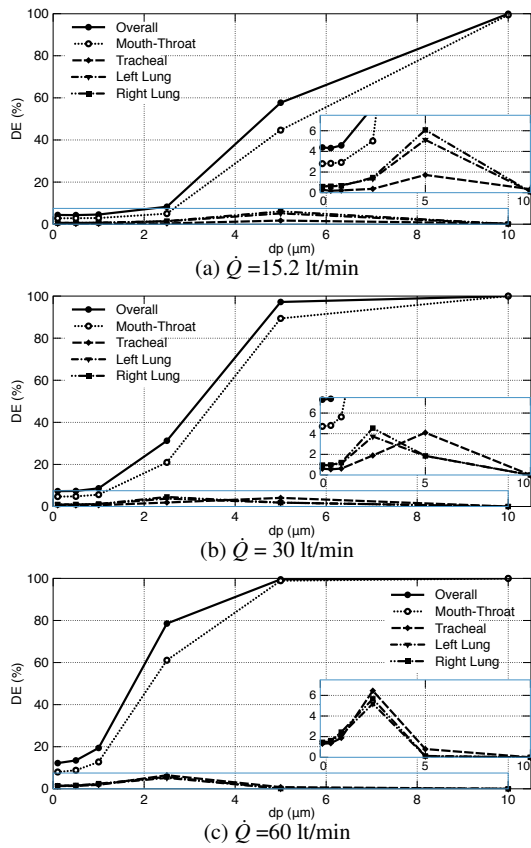


Figure 5: DE under different flowrates (healthy lungs,  $q=0$ ).

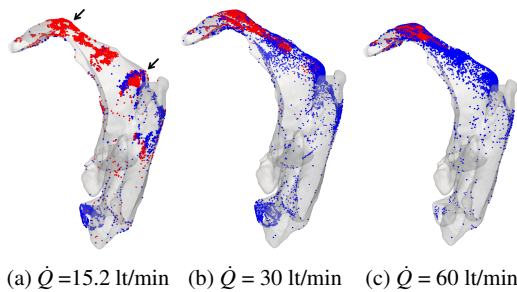


Figure 6: Deposition locations of 5 (blue) and  $10\mu\text{m}$  (red) particles in the Mouth-Throat region under different flowrates (healthy lungs,  $q=0$ ).

$\mu\text{m}$  particles and therefore such a high charge level on these particles might unrealistic. On the other hand, charge levels of 250 elementary charges for these smallest particles, which is feasible charge value, are found to enhance deposition by a factor of 2 in generations 0–7 of the airway tree, thus reducing the number of exhaled out particles, in the case of therapeutic purposes. The enhancement in deposition is expected to be even greater deeper in the lungs as a result of the smallest diameters and greater residence times, rendering the use of nano sized particles promising for efficient pulmonary drug delivery. Future studies on the current topic are therefore recommended. The impact of charge becomes less significant as the particle size is increased: overall DE

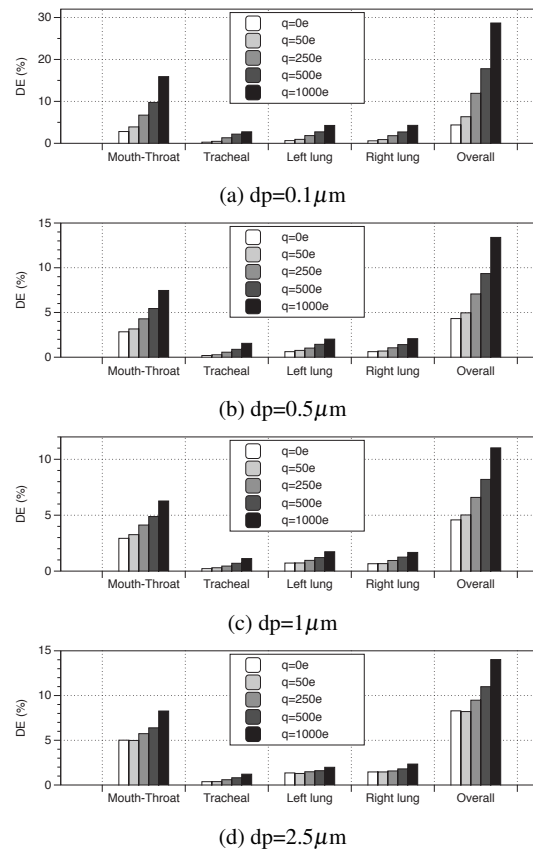


Figure 7: Overall and sub-regional DE of particles with different charge levels ( $\dot{Q} = 15.2$  lt/min).

of 0.5, 1 and  $2.5\mu\text{m}$  particles with 1000 elementary charges are approximately 3, 2 and 1.5 times greater than that with no charge respectively. For all particles sizes, most of the deposition enhancement occurs in the mouth-throat region. The distribution of deposition enhancement in this region is mostly uniform and results from the narrow passage from mouth inlet to the entrance of oral cavity and large residence times in the oropharynx and the laryngopharynx, due to both low velocities and recirculation regions. Also, many charged particles are trapped and deposited in the blocked nasopharynx. The deposition enhancement in this region could be decreased in some extent if it is unwanted (e.g. in the case of drugs intended for systemic uptake) by combining a mouth-piece, which can increase the hydraulic diameter in the region of the tongue, and a higher flowrate, which will reduce residence times in the laryngopharynx region. This is also an important issue for future research studies.

**Effect of physiology** As previously mentioned, the effect of obstructed airways on particle deposition characteristics was examined by reducing the luminal areas of lower airway generations using a scaling factor  $\alpha = d_0/d = 1.5$ . In the upper extrathoracic region, airway obstruction was not found to have a significant impact on the airflow and particle transport and deposition. However, in the lower bronchial generations, the luminal area reduction induced significantly higher local airflow velocities, which in turn resulted in greater deposition due to impaction, as shown in DE plots of fig. 8 for the Left and Right lung regions. The in-

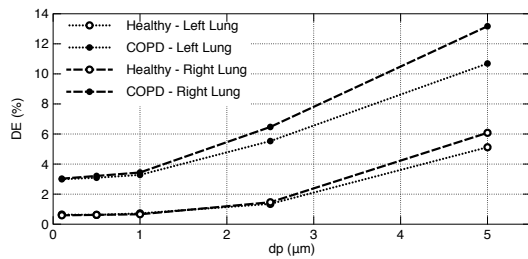


Figure 8: DE for healthy and COPD lungs in left and right lung regions ( $\dot{Q}=15.2$  lt/min,  $q=0$ ).

crease in DE is more pronounced for larger particles (larger Stokes numbers) for which it is more difficult to avoid obstacle surfaces such as bifurcations (absolute values of DE are more than doubled for 2.5 and 5 μm particles in the lower airways). The relative increases in DE ( $\frac{DE_{Healthy}-DE_{COPD}}{DE_{Healthy}}$ ) for particles 0.1, 0.5 and 1 μm for left/right lung regions are 367/414 %, 400/418 % and 355/421 % respectively. The current results show that for pulmonary drug delivery purposes in COPD diseased lungs care must be taken in assessing sufficient dosimetry for medicinal treatment.

## CONCLUSIONS

LES were used to investigate the transport and deposition of inhaled aerosol particles in a realistic geometry of the human lungs reconstructed from CT-scans under three steady inhalation flowrates. The effects of aerosol charge and lower generation airway narrowing caused by COPD on particle deposition were also examined. Specific conclusions are:

- The mean flow structures at the three flowrates are qualitatively similar regardless of Reynolds number. Similar swirling motions are generated from the impingement of the laryngeal jet on the tracheal front wall. The locations of maximum TKE in the oral region differ as the flowrate is varied due to different dispersion characteristics of the oral jet. Greater values of turbulent intensities that persist further downstream in the trachea and the main bronchi are observed at higher flowrates.
- The DE of particles is increased with flowrate due to greater inertial impaction. The effect of flowrate is more pronounced on the deposition of 2.5 and 5 μm diameter particles (enhanced deposition in the mouth-throat region), while 0.1, 0.5 and 1 μm diameter particles have similar DE at a given flowrate.
- The effect of charge is more significant for smaller particles; the overall DE of 0.1 μm with 1000 elementary charges is approximately 7 times greater than that with no charge. The findings of this study indicate that by manipulating electrostatic charge, it is possible to increase deposition in certain regions, presenting an opportunity for maximizing the therapeutic outcome. Future studies on the use of charged particles for increasing efficacy of pulmonary drugs are therefore recommended.
- Obstructed lower generation airways result in enhanced deposition due to inertial impaction. This must be considered when assessing pulmonary drug dosimetry for COPD patients.

## ACKNOWLEDGEMENTS

The present study was funded by the European Union 7th framework program HEXACOMM FP7/2007-2013 under grant agreement N<sup>o</sup> 315760.

## REFERENCES

- 2008 *World Health Statistics*. World Health Organization.
- Ali, M., Reddy R.N. Mazumder M. K. 2008 Electrostatic charge effect on respirable aerosol particle deposition in a cadaver based throat cast replica. *Journal of Electrostatics* **66**, 401–406.
- Choi, J., Tawhai, M.H., Hoffman, E.A. & Lin, C.-L. 2009 On intra- and intersubject variabilities of airflow in the human lungs. *Phys. Fluids* **21** (101901).
- Forsyth, B., Liu B.Y. H. Romay F. J 1998 Particle charge distribution measurement for commonly generated laboratory aerosols. *Aerosol Science and Technology* **28**, 489–501.
- Hasegawa, M., Nasuhara Y. Onodera Y. Makita H. Nagai K. Fuke S. Ito Y. Betsuyaku T. Nishimura M. 2006 Airflow limitation and airway dimensions in chronic obstructive pulmonary disease. *American Journal of Respiratory and Critical Care Medicine* **173** (12), 1309–1315.
- Johnstone, A., Uddin, M., Pollard, A., Heenan, A. & Finlay, W. H 2004 The flow inside an idealised form of the human extra-thoracic airway. *Experiments in Fluids* **37**, 673–689.
- Kim, C. S. & Kang, T. C. 1997 Comparative measurement of lung deposition of inhaled fine particles in normal subjects and patients with obstructive airway disease. *American Journal of Respiratory and Critical Care Medicine* **155**, 899–905.
- Kwok, P. C. L., Glover W. Chan H. K. 2005 Electrostatic charge characteristics of aerosols produced from metered dose inhalers. *Journal of Pharmaceutical Sciences* **94** (12), 2789–2799.
- Kwok, P. C. L. & Chan, H. K. 2009 Electrostatics of pharmaceutical inhalation aerosols. *Pharmacy and Pharmacology* **61**, 1587–1599.
- Kwon, S. J. & Seo, I. W. 2005 Reynolds number effects on the behavior of a non-buoyant round jet. *Experiments in fluids* **38**, 801–812.
- Lin, C.-L., Tawhai, M.H., McLennan, G. & Hoffman, E.A. 2007 Characteristics of the turbulent laryngeal jet and its effect on airflow in the human intra-thoracic airways. *Respiratory Physiology and Neurobiology* **157**, 295–309.
- Luo, H.Y. & Liu, Y. 2008 Modeling the bifurcating flow in a ct-scanned human lung airway. *Journal of Biomechanics* **41** (12), 2681–2688.
- Prodi, V., Mularoni A. 1985 Electrostatic lung deposition experiments with humans and animals. *Annals of Occupational Hygiene* **29** (229-240).
- Radhakrishnan, H. & Kassinos, S. 2009 Cfd modeling of turbulent flow and particle deposition in human lungs. Minneapolis, Minnesota, USA.
- Schiller, L. & Naumann, Z. 1935 *Ver. Deutsch Ing.*
- Weibel, E.R. 1965 *Morphometry of the human lung*. Springer.
- Xi, J. & Longest, P. W. 2007 Transport and deposition of micro-aerosols in realistic and simplified models of the oral airway. *Annals of Biomedical Engineering* **35**, 560–581.
- Yu, C.P. 1985 Theories of electrostatic lung deposition of inhaled aerosols. *Annals of Occupational Hygiene* **29**, 219–227.